Unstructured LES_{DNS} of a Turbulent Boundary Layer over a Gaussian Bump

James R. Wright*, Riccardo Balin*, John A. Evans†, Kenneth E. Jansen‡
University of Colorado Boulder, Boulder, Colorado 80309

Wall-resolved large eddy simulation (WRLES) is often thought to have mesh resolution requirements that grow at the same asymptotic rate as direct numerical simulation (DNS), but WRLES actually does grow slower than DNS, even if the near-wall region is resolved to DNS resolution. In this paper, a new simulation concept dubbed LES_{DNS} is undertaken, where the near-wall and inflow resolution of a WRLES is taken down to DNS levels. The primary advantage of this approach is that it removes the need for sub-grid models in the highly-anisotropic near-wall region, where they are the least mature. When combined with the use of unstructured grids that coarsen in all three directions outside of this near-wall region, significantly higher Reynolds numbers may be simulated for wall-bounded flows relative to traditional DNS. In this work, LES_{DNS} is applied to the zero pressure gradient flat plate boundary layer and Gaussian bump problems. The new concept was found to be effective for both cases tested. In particular, LES_{DNS} of the Gaussian bump was able to closely match DNS results at a fraction of the cost despite the complex physics involved with the problem. It is found that the new concept is effectively able to provide the sub-grid stress model with a "perfect wall model". Because of this "perfect wall model", deficiencies in the standard dynamic sub-grid stress model were identified in the outer region of the boundary layer in the Gaussian bump case.

I. Nomenclature

C_f	=	coefficient of friction
C_p	=	coefficient of pressure
Δ	=	grid resolution
δ	=	boundary layer height
k	=	turbulent kinetic energy
ν	=	dynamic viscosity
ν_t	=	eddy viscosity
L	=	characteristic length of Gaussian bump
Re_θ	=	momentum thickness Reynolds number
S_{ij}	=	strain rate tensor
S	=	strain rate magnitude, $\sqrt{2S_{ij}S_{ij}}$
U_∞	=	reference freestream velocity
u_τ	=	friction velocity, $\sqrt{\tau_w/\rho}$

Superscripts

$+$	=	normalized by wall units
$'$	=	fluctuating component

Subscripts

*Graduate Research Assistant, Ann and H. J. Smead Department of Aerospace Engineering Sciences. Student Member AIAA.
†Assistant Professor, Ann and H. J. Smead Department of Aerospace Engineering Sciences. Senior Member AIAA
‡Professor, Ann and H. J. Smead Department of Aerospace Engineering Sciences. Associate Fellow AIAA.

in = inlet values
n = wall-normal component
s = streamwise component, tangent to wall
z = spanwise component

II. Introduction

While the continued improvement of computer resources for computational fluid dynamics (CFD) has enabled the simulation of a number of flows with highly accurate direct numerical simulations (DNS), these flows are still limited to relatively low Reynolds numbers and mostly focus on simpler canonical physics [1–6]. By contrast, many engineering flows that require the use of reliable turbulence modeling experience significantly larger Reynolds numbers and a larger degree of complexity [7–11]. This disparity between the high-fidelity data available and the flows of interest to engineers limits the value of such DNS.

A reduction in the computational cost of the simulation is achieved by performing large eddy simulation (LES), wherein only the larger eddies responsible for the majority of the turbulent transport are resolved, while the effects of the small and unresolved scales are modeled. With LES, higher Reynolds number flows can be computed [12], however a model must be used to represent the scales that are not resolved (sub-grid scale model). Sub-grid scale (SGS) models are relatively more mature and better understood for the isotropic regions of the flow found in the outer part of the boundary layer, but are less so for the anisotropic scales encountered in the near-wall region [13–15]. As a consequence, while LES extends the reach of scale resolving simulations to larger Reynolds numbers, the accuracy of the computation is sometimes negatively impacted by the inaccuracies of SGS modeling near the wall [16].

The purpose of this study is to use a mixed DNS and LES approach, heretofore referred to as LES_{DNS} , in order to achieve a level of accuracy similar to DNS while keeping the cost of the simulation only slightly larger than wall-resolved LES (WRLES). The LES_{DNS} framework is most similar to a WRLES, but with the suspect inner layer region (i.e. $y^+ < O(100)$ or $y/\delta < 0.1$) refined to DNS resolution such that all scales are resolved and the SGS modeling is shut off. Effectively, DNS is performing the role of the "perfect" wall model for the LES region above it. Perfect is in quotes because the claim is subject to the fact that the DNS layer is being driven by the LES above it. To the extent that the structures close to the wall are not too strongly influenced by the small scale structures away from the wall, it is perfect. Furthermore, the term "model" is used loosely because in fact no modeling is being performed in the DNS resolved near-wall region. While it is a commonly held belief that meshes required for WRLES grow at the same rate as DNS (10/4 power of the Reynolds number), this is not the case. Even a WRLES that refines to DNS resolution below a $y+ = O(100)$ has an asymptotic mesh growth rate 3/4 lower (e.g., 7/4 power as observed in Fig. 1). The lower growth rate is due to the fact that, as the Re is increased, the portion of the boundary layer that requires this fine resolution is of fixed size while the portion that requires much coarser outer layer LES resolution continues to grow. This is plainly seen in the behavior of the wall-normal spacing. For DNS, it is capped at 6-12 plus units while an LES can allow it to grow geometrically until it reaches the outer layer scale (typically $\delta/20$ - $\delta/64$). The key value in using this LES_{DNS} approach is thus that, due its lower growth rate, it can be applied to significantly higher Reynolds numbers than DNS and thus broaden the range of Reynolds number effects that can be studied under a fixed computational resource while maintaining a high level of accuracy. Another significant benefit is that it isolates the inner and outer regions of the boundary layer, enabling the evaluation and improvement of SGS closures in the outer layer of complex flows when the inner layer is computed with DNS accuracy. Finally, it provides DNS-quality data for the inner layer at higher Reynolds number which is not only essential to understanding the fundamental physics but also to evaluate and improve lower-fidelity closures in this region for WRLES, wall-modeled LES (WMLES), and Reynolds-averaged Navier-Stokes (RANS) simulations [6, 17, 18].

For testing LES_{DNS} , a turbulent boundary layer over a planar bump geometry seems a natural choice. It provides a succession of pressure gradients in addition to subjecting the flow to geometric effects. There are many bump geometries popular in numerical simulation, including the NASA wall-mounted hump [19], which has been studied in DNS [20], WRLES [16, 21], and WMLES [22], and the parametric circular bump [23], which was recently studied in [17] for a family of bumps using WRLES. For this paper, the Gaussian bump [24] will be used for testing the LES_{DNS} concept. It is being studied experimentally [25] and has been the subject of DNS, LES, and RANS computations [9, 26, 27]. An overview of the flow physics is given in Section III.B. The SGS model selected for LES_{DNS} was the standard dynamic Smagorinsky model [13, 28], which has been successfully used for other bump WRLES simulations [17, 21]. In addition to the Gaussian bump, an LES_{DNS} simulation of a zero pressure gradient (ZPG) flow over a flat plate is also studied. The latter provides a validation of LES_{DNS} on a simple, well understood flow, while the bump will fully test the

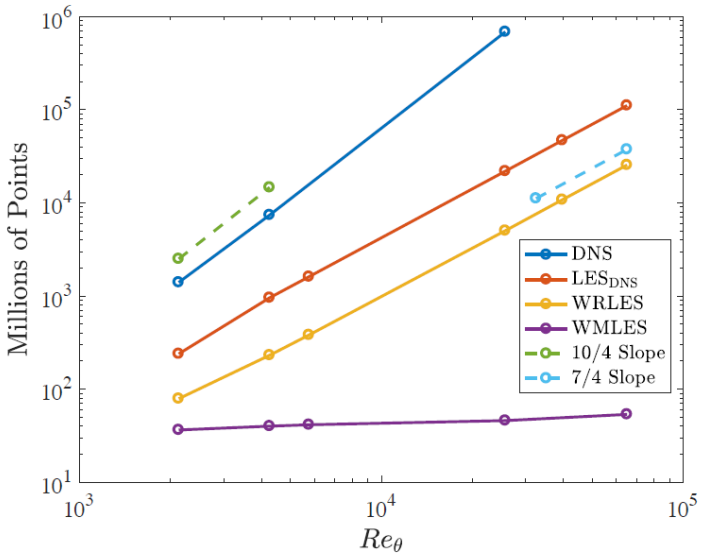

Fig. 1 Mesh sizes required with various scale resolving simulation approaches as a function of Re_θ for a bump flow with domain $70\delta_{in}$ long and $10\delta_{in}$ wide.

paradigm and it's potential cost savings.

III. Computational Setup and Flows Studied

A. LES_{DNS} Method

For an LES_{DNS} approach, the grid resolution is critical as, with the use of the dynamic model, it will effectively designate where the DNS and LES regions of the domain are. As such, there are three main layers of the grid: the inner layer, outer layer, and free-stream. The inner layer will contain DNS resolution, while the outer layer will be LES resolution. Finally, the grid may be coarsened further in the free-stream where no turbulence structures exist and only inviscid flow gradients need to be resolved. Changes in resolution were achieved smoothly using an unstructured grid composed of tetrahedral elements.

For the simulations considered in this paper, the inner layer mesh will extend up to $n^+ \approx 80$, where n is the wall-normal direction. The inner layer resolution will be normalized to local wall-friction units. For the meshes in this paper, precursor RANS simulations are used to estimate the local wall-friction* when translating from the targeted wall-friction-normalized resolution to physical mesh resolution. The outer layer was extended twenty percent higher than the RANS boundary layer thickness to account for intermittency of the super-layer. The outer layer mesh starts at the top of the inner layer and therefore matches the DNS resolution. However, as it progresses away from the wall, the normal mesh resolution stretches to no larger than $\Delta n_{max} = \delta/64$ to maintain adequate resolution for LES in that region. The wall-parallel grid spacing may also expand in this region to roughly the same size as the normal spacing since isotropic eddies are expected. Finally, the free-stream further coarsens outside of the outer layer. Note, by coarsening in all three dimensions very smoothly (growth rates of one percent in the streamwise direction and five percent in the normal direction), LES resolution of the outer layer is gradually achieved. This mesh design results in an unstructured LES_{DNS} grid with far fewer elements than a DNS while matching its near wall resolution. Collectively, these features allow LES_{DNS} to extend to much higher Reynolds numbers than DNS and while remaining free of near-wall SGS modeling limitations.

The standard dynamic Smagorinsky model is used as the SGS model [13, 28]. It is known that as the grid size approaches the Kolmogorov length scale, the standard dynamic model will over-predict the Smagorinsky coefficient, leading to excess eddy viscosity, ν_t [29]. Therefore, to make the simulation be true to the spirit of the LES_{DNS} concept,

*A limiter on the wall-friction is used so that unreasonably coarse meshes are avoided in regions of ill-defined wall-friction in the vicinity of flow separation.

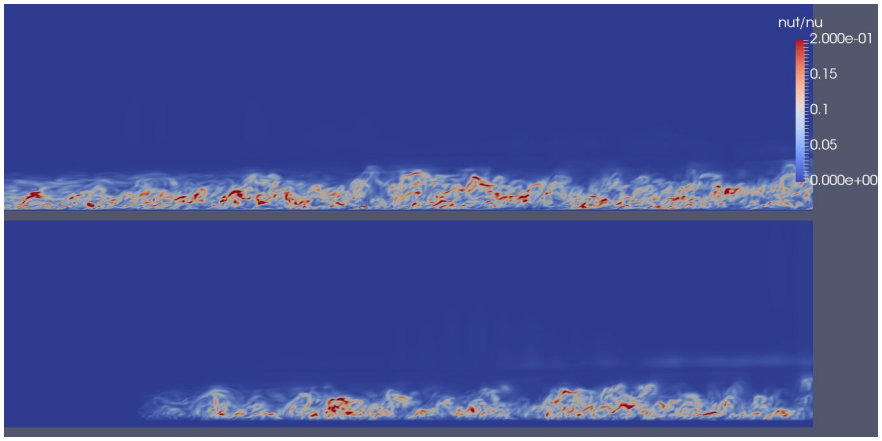

Fig. 2 Comparison of using ν_t suppression in the STG development region and the near-wall region. The top is without ν_t suppression and the bottom with suppression. The contour shown is instantaneous ν_t/ν.

the ν_t value is forced to zero in the near-wall region ($n^+ < 40$). This was also done across the entire boundary layer thickness in the development region ($5\delta_{\text{in}}$) downstream of the inflow boundary condition to ensure a satisfactory transition to "natural" turbulence. The synthetic turbulence generator (STG) of [30] was used to generate unsteady velocity fluctuations, which was shown to be effective in a number of studies [27, 31–33]. The progression from these forced $\nu_t = 0$ regions to the dynamic-model-determined ν_t is done by a linear ramp over 40 plus units in the wall-normal direction for the near-wall region and over $3\delta_{\text{in}}$ in the streamwise direction for the STG development region. The result of this suppression of ν_t can be seen in Fig. 2.

B. Gaussian Bump

The primary flow problem selected for this work is a turbulent boundary layer over the prismatic extrusion of a two-dimensional Gaussian bump, shown in Fig. 3 by the black curve on the lower surface of the domain. This flow was studied using RANS, WMLES, and DNS in [27, 33], and a detailed explanation of the problem setup and geometry is found therein. Note that a separate DNS simulation of the same Gaussian bump flow was also done by Uzun and Malik [26], however differences at the inflow boundary condition result in the two simulations being distinct. Moreover, it is important to mention that the profile of the bump being considered here is exactly the centerline of another fully three-dimensional bump [24] and being studied experimentally in a collaboration between the University of Washington and The Boeing Company [25].

The Reynolds number defining the flow is $Re_L = 1.0\text{M}$, where L is the characteristic length of the Gaussian bump of 3 ft (0.9144 m) as well as the width of the 3D wind-tunnel geometry studied in [25]. This corresponds to a Reynolds number based on the bump height of $Re_h = 85,000$. The free-stream velocity (U_∞) is approximately 16 m/s, resulting in a small enough Mach number ($M_\infty < 0.05$) to treat this flow as incompressible. The origin of the turbulent boundary layer is located at $x/L = -1$ (a distance of L upstream of the peak of the bump), producing a boundary layer with thickness shown by the green curve over the bump surface in Fig. 3. At the location of the inlet to the scale resolving simulations (shown by the dotted line in Fig. 3), the momentum thickness Reynolds number is $Re_\theta = 1,050$, and the boundary layer thickness is about $1/8$ of the bump height (corresponding to $\delta_{\text{in}}/L = 0.0094$).

In order to reduce the cost of the scale resolving simulations of the bump, the computational domain and boundary conditions are altered relative to the description in Fig. 3 as follows. The inflow plane is located at $x/L = -0.6$ (dotted line in Fig. 3), where the adverse pressure gradient (APG) upstream of the bump is weak, and the outflow is placed at $x/L = 1$. The spanwise period of the domain is $L_z = 4\delta_{\text{in}}$. Due to the growth of the boundary layer on the downstream side of the bump, this width introduces some confinement effects on the solution. However, these effects are small for $x/L < 0.1$, which is the primary region of interest of this paper (i.e. the strong favorable and early adverse pressure gradient on the downstream side of the bump). The top boundary is modeled as an inviscid wall and is slanted according to a profile fitted to the displacement thickness of the top boundary layer computed with the preliminary RANS simulation of the entire geometry (see Fig. 3). This was done to reproduce the constriction effects of the boundary layer growing on the top surface.

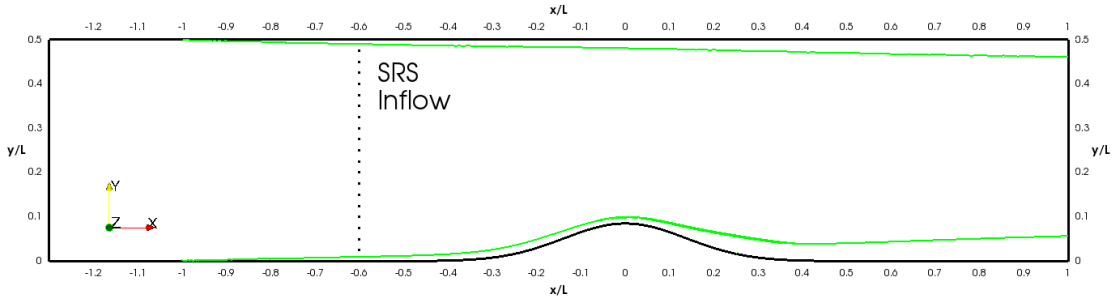

Fig. 3 The black curves outline the computational domain defining the flow, while the green curves show the boundary layer thickness predicted with RANS [33] on both no-slip walls using an isoline of spanwise vorticity. The dotted vertical line shows the location of the unsteady inflow to the scale resolving simulations (SRS). Reproduced from [33].

As discussed in detail in [27], the boundary layer over the Gaussian bump is subjected to a plethora of fluid flow phenomena. In addition to a series of strong pressure gradient and streamline curvature effects, the flow also experiences an incomplete relaminarization process caused mainly by the strong favorable pressure gradient (FPG) accelerating the flow on the upstream side of the bump, and a partial retransition taking place at the bump peak where the pressure gradient rapidly switches from favorable to adverse. These individual effects combine to create complicated flow physics with significant deviation from standard turbulence behavior, as described below.

During relaminarization, the near-wall region of the boundary layer gradually ceases to be fully turbulent and spots of quiet flow appear throughout the inner layer. Relaminarization does not complete however, thus a quasi-laminar state is not achieved. Under this process, the streamwise velocity deviates significantly above the logarithmic law. As the viscous layer grows thicker, the Reynolds shear stress is reduced (especially when non-dimensionalized by the local friction velocity) and takes a bi-modal shape, and the skin friction coefficient drops while the flow is still being accelerated. By contrast, the outer layer remains fully turbulent, although the fluctuations are significantly suppressed by the acceleration and the convex curvature.

In the vicinity of the bump peak, where the pressure gradient changes sign, the near-wall flow weakened by the upstream acceleration experiences a sudden enhancement in turbulent intensity brought about by the retransition process. Spots of large vorticity appear at the wall, and a surge in turbulent kinetic energy and Reynolds shear stress is exhibited in the inner layer. The skin friction is also increased, resulting in a local minimum and maximum in rapid succession. A new highly energetic internal layer is formed which is more resilient to the strong APG and only develops incipient separation on the downstream side of the bump. By contrast once again, the turbulence fluctuations in the outer layer decay further under the continued convex curvature effects which persist throughout the APG region, causing the Reynolds shear stress to change sign.

The boundary layer over the Gaussian bump at the Reynolds number chosen is therefore both a challenging and exciting test case for the LES_{DNS} modeling paradigm. The strong favorable and adverse pressure gradients lead to complex near-wall physics that are critical to the skin friction coefficient profile over the surface. For instance, the extent of flow separation on the leeward side depends heavily on the development of the internal layer through the APG, and thus on the retransition and relaminarization processes occurring upstream. All of these phenomena will challenge the idea of a "perfect DNS wall model". Moreover, the outer layer turbulence exhibits significant changes due to the convoluted interaction of pressure gradient and curvature effects, thus providing a challenge to the LES SGS model.

C. Zero Pressure Gradient Flat Plate

Before tackling the full Gaussian bump simulation, a zero pressure gradient (ZPG) flat plate boundary layer is used to validate the LES_{DNS} concept. To ensure that this simulation is relevant to the bump case, the flow conditions at the inflow are matched. The only difference in the extruded geometry between this case and the bump is that the curved bump floor is replaced by a flat plate and the top boundary is replaced by an inclined surface that allows an outflow boundary condition to be applied. Together, these changes ensure that ZPG is achieved. The domain size was chosen to be $13\delta_{\text{in}}$ long and $2\delta_{\text{in}}$ wide.

D. General Computational Setup

At the inflow of all of the scale resolving simulations presented in this paper, the synthetic turbulence generator described in [30] was selected to introduce unsteady flow into the domain. According to this approach, the velocity fluctuations are first created from a superposition of spatiotemporal Fourier modes with random amplitudes and phases, and are then scaled by prescribed profiles of time-averaged Reynolds stresses in order to obtain the proper second order moments. The fluctuations are finally added to a mean velocity profile to obtain the spatially and time-varying boundary condition.

For the Gaussian bump simulations, the mean Reynolds stress and velocity profiles required by the method are extracted from a preliminary RANS simulation at the inflow location of $x/L = -0.6$ (see Fig. 3). The details of this preliminary RANS are described in detail in [27, 33]. For the ZPG flat plate, the inflow mean profiles were also taken from a RANS simulation. In this case, the simulation matched the freestream conditions of the Gaussian bump and also resolved the boundary layer origin as shown in Fig. 3. Given the low Reynolds number of the flow, the Spalart-Allmaras closure [34] with the correction of [6] was used in order to obtain accurate skin friction at the inflow.

It should be noted that [35] provides a means to assess and improve the convergence of the STG method to these target inflow profiles via careful choice of the random numbers upon which it depends. This paper also documents that some choices of random numbers can yield stresses up to 40% off their target. However, since the DNS results of [27] predated this paper, the LES_{DNS} results discussed here did not follow the random number optimization procedures of [35] but instead used the same random numbers and start time (phase) as [27] ensuring all comparative simulations had the exact same inflow conditions. It should be stressed that comparing simulations that use STG inflow methods without taking care to assess how well the statistics of the inflow agree is ill advised.

Lastly, all the simulations were run using the Parallel-Hierarchic-Adaptive-Stabilized-Transient-Analysis (PHASTA) flow-solver. It is an open-source, stabilized, implicit finite element solver [36] for either the incompressible or compressible Navier-Stokes equations plus any modeling equations and terms. Streamline-upwind Petrov-Galerkin (SUPG), pressure-stabilizing Petrov-Galerkin (PSPG), and grad-div stabilization were used [36]. Time integration is done using the generalized-α method [37]. All meshes for LES_{DNS} discussed in this study used tri-linear tetrahedral elements.

IV. Numerical Results and Discussion

A. Zero Pressure Gradient Flat Plate

To study the efficacy of the LES_{DNS} concept, simulations were first performed on ZPG flat plate boundary layers. This allowed a reduction in the complexity and computationally expense relative to the Gaussian bump, and further allowed the results to be validated against a number of studies present in the literature. It is important to note that, when using STG at the inflow, a second resolution question is raised – how much resolution is required to obtain a grid independent inflow condition? This question provides a second dimension to the LES_{DNS} modeling paradigm where very fine grids can be used in all three directions in the region that the synthetic turbulence at the inflow is converted into physical turbulence – typically 3-5 boundary layer thicknesses. Similar to the normal gradation described above, the very fine resolution required by STG can be relaxed gradually in the streamwise resolution. Indeed, it is our observation that a grid-independent STG conversion requires streamwise and spanwise grids that are even finer than typical fully developed DNS resolution. For example, while we obtain a grid independent solution when using $\Delta_x^+ = 10$ vs. 15 and $\Delta_z^+ = 4$ vs. 6 for fully developed boundary layer DNS, there was an observable difference in the C_f curves within the first 3 boundary layer thicknesses after an STG inflow (not shown in this paper). To be clear, this difference goes away quickly (almost negligible by 5 boundary layer thicknesses and gone by 10 boundary layer thicknesses). However, since the target application applies STG in a weak but steadily growing adverse pressure gradient, there was concern that the flat plate relaxation to equilibrium could not be relied upon. A more complete study of grid independence of STG is underway in a follow-on paper but, since the use of unstructured grids keeps the cost of a very fine inflow region to about 10% of the total mesh, in this study, mesh sizes that were even finer than those needed for fully developed DNS were used: $\Delta_x^+ = 5$ and $\Delta_z^+ = 2$ over the first three boundary layer thicknesses. After three boundary layer thicknesses, the span and streamwise resolution was allowed to grow slowly (geometric growth rate of one percent) until it reached a value of $\Delta_x^+ = 10$ and $\Delta_z^+ = 6$ which were maintained throughout the DNS region for the remainder of the domain.

As noted earlier, this fine DNS resolution is maintained up to a local normal plus unit of 80 above which the grid is coarsened gradually towards an isotropic mesh once the normal spacing grows to the level of the span and streamwise resolution. Since the normal resolution continues to grow until it reaches $\Delta_n < \delta/64$, the stream and spanwise spacing

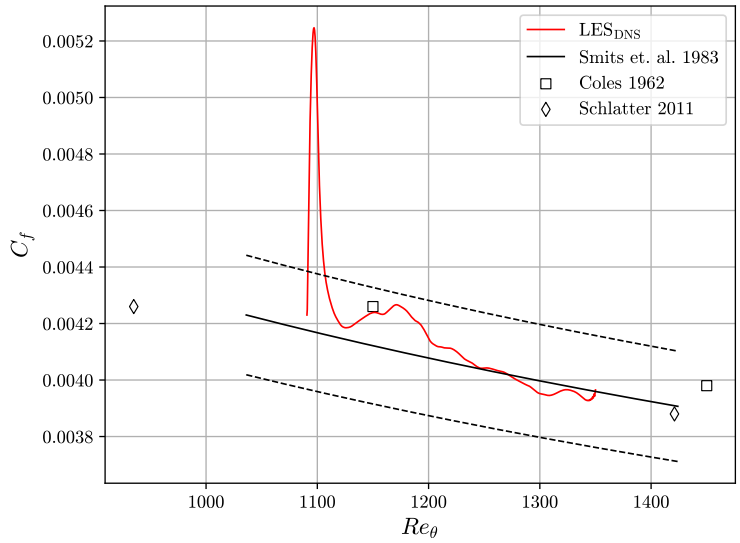

Fig. 4 C_f of flat plate boundary layer using an LES$_{DNS}$ mesh. The thin solid line are the empirical correlations from [39] and the dashed lines surrounding it represent +/- 5% of the empirical value. Also presented are results from [40, 41].

also grow to this level which is generally considered fine enough [38] for the outer layer of LES regions. It should be noted that a structured grid with the same resolution would raise the simulation cost by a factor of six or more. The coefficient of friction for the simulation is plotted in Fig. 4 with respect to Re_θ, with results from other studies also plotted for validation purposes [39–41]. These results show that the unstructured grid design of the LES$_{DNS}$ does adequately predict the skin friction relative to the external validation results.

B. Gaussian Bump

The mesh parameters in local wall-friction units for the LES$_{DNS}$ bump were identical to those given for the flat plate mesh described in the previous section. The initial conditions for the simulation were interpolated from the DNS presented in [27, 33]. The simulation was run until statistical convergence of the flow upstream of separation was achieved. The convergence is demonstrated in Fig. 5. The only significant changes in the differing time windows are at the retransition region ($x/L \approx 0.02$–0.05) and downstream. Ongoing simulations have confirmed that, like the STG region discussed above, the re-transition region requires finer resolution to obtain a grid-independent result. This may be due in part to the dynamic model's poor performance in transitional flows [42, 43], which could require refinement in this region up to DNS to obtain a grid-independent solution. The results that include refinement of this region will be published in later papers but this paper will confine its discussion to the results upstream of retransition $x/L < 0.02$.

The results hereafter are compared to the DNS simulation runs presented in [27], and the RANS and WMLES results from [33]. The RANS result uses the Spalart-Allmaras (SA) model [34] with two model corrections added: rotation and streamline curvature correction [44], and a low Reynolds number correction [6]. The WMLES is an improved delayed-detached eddy simulation using SA (IDDES-SA) as the underlying RANS model operating in WMLES mode [31, 45]. The IDDES is described in detail in [33]. Note that the IDDES model does not utilize the model corrections that the RANS model uses. Quantities of interest are given as their time and spanwise average. A comparison of C_f and C_p is shown in Fig. 6. For C_p, all the simulations return very similar results, with the only major differences being in the incipient separation region (approximately $0.15 < x/L < 0.35$) which is outside of the region of interest to this paper.

For C_f, there are far stronger differences between the simulations. In the mild APG region ($x/L < -0.3$), LES$_{DNS}$ and DNS agree quite well in C_f. After the initial STG C_f spike (which is known to be different for wall resolved methods vs. wall-modeled methods), IDDES-SA and RANS track together and underpredict the DNS C_f for most of this region. From the start of the strong FPG region ($x/L = -0.3$) to DNS's peak C_f value, LES$_{DNS}$ and DNS again correlate quite strongly in C_f. IDDES-SA agrees with the DNS, though not quite as strongly as LES$_{DNS}$.

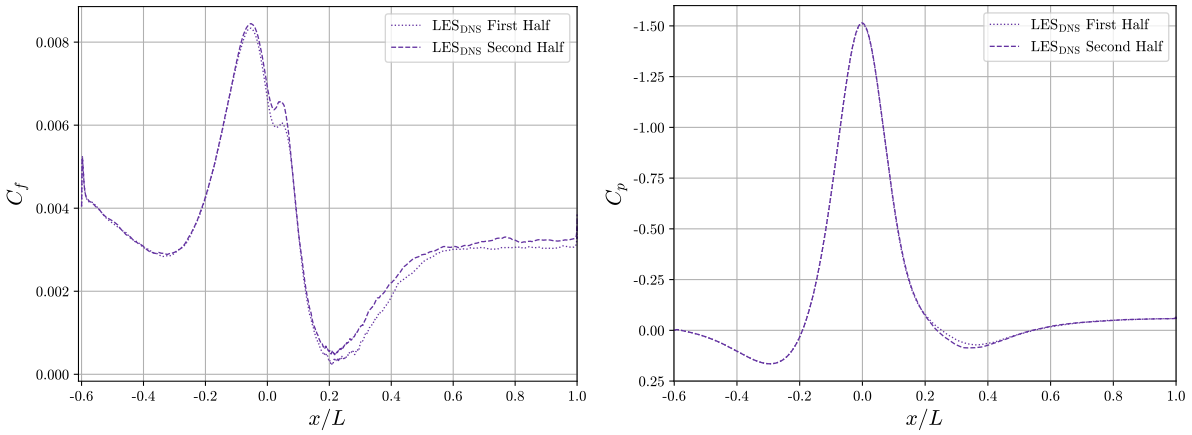

(a) **(b)**

Fig. 5 (a) C_f and (b) C_p plots of LES$_{DNS}$ bump simulation comparing the first and second half of the full statistical window.

Conversely, RANS has a significant overprediction of peak C_f. After the peak C_f value, IDDES-SA begins to drop under both DNS and LES$_{DNS}$. It does feature the local C_f minima and maxima characteristic of the boundary layer retransition, but it's magnitude is quite far off. Until the retransition region ($x/L \approx 0.02$–0.05), LES$_{DNS}$ continues to track very closely to DNS.

Profiles were extracted at various locations before retransition to examine the velocity and Reynolds stress behavior. These profiles were taken in the wall-normal direction, n. The velocity and Reynolds stress are rotated to a wall-oriented orthogonal coordinate system (s, n, z), where s and z are tangent to the bump surface and s is in the streamwise direction. Additionally, to estimate the 99.5% boundary layer height, we use integrated vorticity method

$$\widetilde{U}(s,n) = \int_0^n \overline{\omega_z}(s,n^*)\,\mathrm{d}n^* \qquad \widetilde{U_e}(s) = \widetilde{U}(s, n \to \infty)$$

and define $\widetilde{\delta}_{995} = 0.995\widetilde{U_e}$. This definition has previously been used successfully for flows with non-zero and changing pressure gradients in [2, 26, 27].

Profiles of streamwise velocity are shown in Fig. 7, normalized by local wall-friction units. Log law, taken as $\ln(n^+)/0.41 + 5.0$, has also been plotted for reference. At $x/L = -0.3$, all simulations reasonably agree with DNS. RANS overpredicts the velocity throughout the entire profile and appears to have a slightly larger slope in the log-law region. IDDES-SA is very close to DNS, matching it's slope in the log-law region, though overpredicting the intercept of the line. LES$_{DNS}$ has the strongest agreement with DNS until the outer region of the boundary layer, where it slightly underpredicts the velocity. At $x/L = -0.1$, RANS has significant underprediction of the wall-friction-normalized velocity, $\overline{u_s^+}$. LES$_{DNS}$ and DNS agree well, with IDDES-SA slightly underpredcting DNS but still quite close. At $x/L = 0$ though, IDDES-SA lifts off of the DNS prediction quite significantly. RANS continues to underpredict relative to DNS, but LES$_{DNS}$ remains in excellent agreement.

Plots of the turbulent kinetic energy (TKE, k) and Reynolds shear stress ($\overline{u_s'u_n'}$) are given in Figs. 8 and 9. For all but RANS, these are of resolved turbulence only. For LES$_{DNS}$, modeled stress was estimated to be less than 0.5% of the resolved stress using $\overline{S_{ij}}\,\overline{\nu_t}$, where S_{ij} is the strain rate tensor. Turbulent kinetic energy is defined as half the trace of the Reynolds stress tensor: $1/2(\overline{u_s'u_s'} + \overline{u_n'u_n'} + \overline{u_z'u_z'})$. For RANS, the Reynolds shear stress is given by $2\nu_t S_{ij}$ and TKE is approximated with $k = \nu_t S/0.3$ as suggested in [30], where S is the strain rate magnitude. Also in these plots are vertical lines denoting the beginning and end of ν_t's linear ramp for LES$_{DNS}$, where the leftmost line denotes $\nu_t = 0$ and the rightmost line is where ν_t reaches the full value prescribed by the standard dynamic Smagorinsky model.

For TKE shown in Fig. 8, LES$_{DNS}$ shows good agreement with the DNS results for all three profiles across the full boundary layer. LES$_{DNS}$ slightly overpredicts the peak k value at all three profiles, but maintains the characteristic shape and magnitude of the profile. IDDES-SA similarly agrees with DNS in the outer region of the boundary layer. For the inner region, it generally underpredicts the DNS-predicted k, with $x/L = -0.3$ being the primary exception. RANS is quite poor for $x/L = -0.3$ while the other two profiles at least share the same general characteristics as the DNS

(a)

(b)

(c)

Fig. 6 Plots of (a) $_5$ and (b) $_?$ for the Gaussian bump. (c) $_5$ plots in the region of primary interest.

(a) (b)

(c)

Fig. 7 Plots of wall-friction-normalized streamwise velocity at select pro le locations. Log law is taken to be ln¹=, º•0•41¸ 5•0.

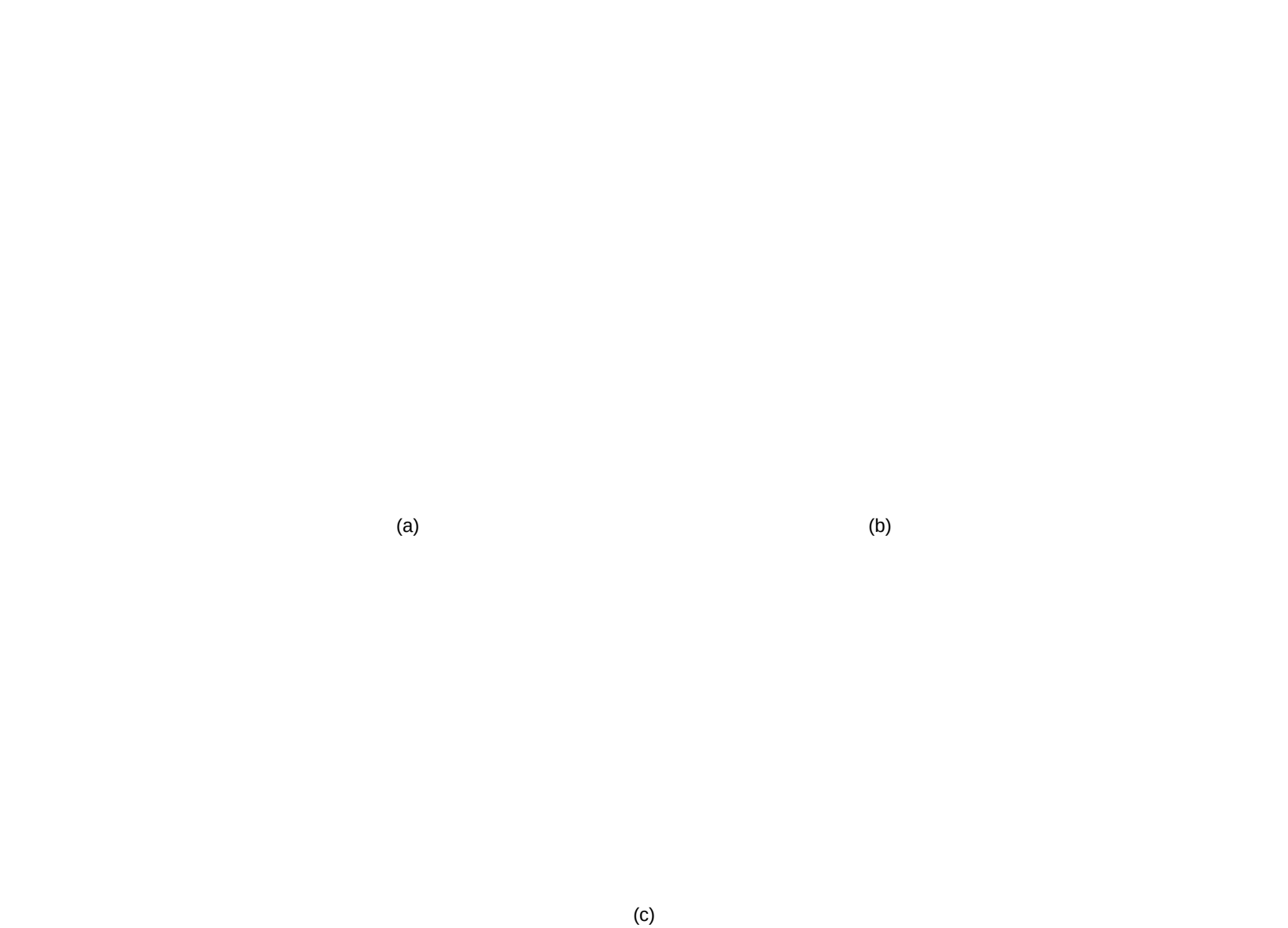

Fig. 8 Plots of turbulent kinetic energy : at select pro le locations. The a_C ramp lines denote the start and stop of the linear ramping of a_C for LES$_{DNS}$. For RANS, : was approximated using $a_C(\bullet 0\bullet 3$, where (is the strain rate magnitude, as suggested in [30].

results. Reynolds shear stress $\overline{\rho}\widetilde{D}''\widetilde{D}''$) tells a similar story. Excluding $G\bullet ! = 0\bullet 3$ (Fig. 9a), RANS is quite far from DNS, IDDES-SA performs well in the outer region, but underpredicts closer to the wall, and LES$_{DNS}$ is in good agreement with the DNS. The primary di erence to the pro les is that LES$_{DNS}$ does not have the overprediction of peak $\overline{\rho}\widetilde{D}''\widetilde{D}''$.

Of note in the : and $\overline{\rho}\widetilde{D}''\widetilde{D}''$ pro les is that for LES$_{DNS}$, the region where the dynamic model is forced o is nearly an identical prediction of the DNS results, sans the overpredicted peak value. This lends credence to the idea that the DNS region of LES$_{DNS}$ is performing as a perfect wall model. It isn't until a_C becomes active that the LES$_{DNS}$ pro les take any signi cant deviation from the DNS. Compare that with the IDDES-SA or RANS results, which deviate from the DNS curves quickly as they move away from the wall. The fact that there is some departure once the LES model becomes active points towards a weakness in the standard dynamic model prediction of the Reynolds shear stress in the outer region of the boundary layer.

V. Conclusions

The LES$_{DNS}$ simulation paradigm was introduced, discussed, and tested. First, an unstructured tetrahedral grid was proven e ective in an LES$_{DNS}$ concept for solving a ZPG at plate boundary layer. An LES$_{DNS}$ simulation was then performed of the Gaussian bump and compared to DNS, IDDES-SA (in WMLES mode), and RANS. The LES$_{DNS}$ result compared well to DNS in conditions traditionally challenging for simulation of turbulent boundary layers, including changing pressure gradients, curvature e ects, and relaminarization. This could be easily seen by the comparative

(a) (b)

(c)

Fig. 9 Plots of Reynolds shear stress $\overline{u'v'}$ at select profile locations. The a_C ramp lines denote the start and stop of the linear ramping of a_C for LES_{DNS}.

RANS and IDDES-SA results. Further, the cost of the LES$_{DNS}$ was signi cantly less expensive than the DNS simulation it is compared to. A full description of the savings is left for the journal paper that follows which will include ner mesh results that adequately resolve the retransition region excluded from discussion in this paper.

The simulation relied upon an STG method to introduce an unsteady in ow with statistics consistent with the RANS solution over a full domain. The unstructured grids used allowed a grid-independent solution of the region where the random uctuations from STG are converted to physical turbulence, further extending the concept of LES$_{DNS}$ to include DNS quality in ow to an LES simulation at modest (10%) additional expense.

Examining the behavior of the LES$_{DNS}$ concept, the simulation results lend credence to the idea of using a DNS near-wall layer as a perfect wall model; before the dynamic model was allowed to become active, LES$_{DNS}$ consistently matched the DNS results. The results also showed the potential for LES$_{DNS}$ to isolate the performance of an SGS model for the outer region of a boundary layer from it's performance in the inner layer. In this particular case, it is shown that the standard dynamic model may have some minor de ciencies in the modeling the outer boundary layer for the Gaussian bump.

On-going are studies to reach grid independence in the retransition region of the ow, with plans on simulating the Gaussian bump at higher Reynolds numbers. Future work on the LES$_{DNS}$ paradigm includes testing other SGS models [29, 46, 47] and extensions to higher Reynolds numbers where the cost savings of LES$_{DNS}$ over DNS become more dramatic.

Acknowledgments

The authors would like to acknowledge the Computational and Data-Enabled Science and Engineering (CDS&E) program of the National Science Foundation (NSF) CBET-1710670, as well as the Transformational Tools and Technologies Project of the National Aeronautics and Space Administration (NASA) 80NSSC18M0147 for funding of this work. Moreover, they thank the NASA High-End Computing (HEC) Program through the NASA Advanced Supercomputing (NAS) Division at Ames Research Center and Argonne Leadership Computing Facility (ALCF), which is a DOE O ce of Science User Facility supported under Contract DE-AC02-06CH11357, for the resources on which the simulations and post-processing were performed. Finally, the authors thank Dr. M. K. Strelets for the helpful communications regarding the STG in ow method.

References

[1] Lee, M., and Moser, R. D., Direct numerical simulation of turbulent channel ow up to $Re_\tau = 5200$, Journal of Fluid Mechanics, Vol. 774, 2015, pp. 395 415.

[2] Spalart, P. R., and Watmu , J. H., Experimental and numerical study of a turbulent boundary layer with pressure gradients, Journal of Fluid Mechanics, Vol. 249, 1993, pp. 337 371.

[3] Spalart, P. R., and Coleman, G. N., Numerical study of a separation bubble with heat transfer, European Journal of Mechanics B/Fluids, Vol. 16, 1997, pp. 169 189.

[4] Na, Y., and Moin, P., Direct numerical simulation of a separated turbulent boundary layer, Journal of Fluid Mechanics, Vol. 374, 1998, pp. 379 405.

[5] Kitsios, V., Atkinson, C., Sillero, J. A., Borrell, G., Gungor, A. G., Jimenez, J., and Soria, J., Direct numerical separation of a self-similar adverse pressure gradient turbulent boundary layer, International Journal of Heat and Fluid Flow, Vol. 61, 2016, pp. 129 136.

[6] Coleman, G. N., Rumsey, C. L., and Spalart, P. R., Numerical study of turbulent separation bubbles with varying pressure gradient and Reynolds number, Journal of Fluid Mechanics, Vol. 847, 2018, pp. 28 70.

[7] Balin, R., Rasquin, M., Chitale, K. C., and Jansen, K. E., Investigation into the performace of turbulence models for the computation of high-lift ows at large angles of attack, AIAA 2017-3563, 2017.

[8] Balin, R., and Jansen, K. E., A comparison of RANS, URANS, and DDES for high-lift systems from HiLiftPW-3, AIAA 2018-1254, 2018.

[9] Balin, R., Wright, J. R., Patterson, J. W., Farnsworth, J., Evans, J., Lakhani, R., Spalart, P. R., and Jansen, K. E., Hybrid turbulence model computations of the NASA juncture ow model using PHASTA, AIAA 2020-1777, 2020.

[10] Jansen, K. E., Rasquin, M., Farnsworth, J. A., Rathay, N., Monastero, M. C., and Amitay, M., Interaction of a synthetic jet with separated ow over a vertical tail, AIAA Journal, Vol. 56, No. 7, 2018, pp. 2653 2668.

[11] Rasquin, M., Farnsworth, J. A., Balin, R., and Jansen, K. E., Modeling strategies of active ow control applied to a vertical tail assembly, AIAA 2020-2944, 2020.

[12] Choi, H., and Moin, P., Grid-point requirements for large eddy simulation: Chapman's estimates revisited, Physics of Fluids, Vol. 24, 2012, p. 011702.

[13] Germano, M., Piomelli, U., Moin, P., and Cabot, W. H., A dynamic subgrid-scale eddy viscosity model, Physics of Fluids, Vol. 3, 1991, pp. 1760 1765.

[14] Härtel, C., and Kleiser, L., Subgrid-scale energy transfer in the near-wall region of turbulent ows, Physics of Fluids, Vol. 6, 1994, pp. 3130 3143.

[15] Piomelli, U., and Yu, Y., Subgrid-scale energy transfer and near-wall turbulence structure, Physics of Fluids, Vol. 8, 1996, pp. 215 224.

[16] Uzun, A., and Malik, M. R., Large-Eddy Simulation of Flow over a Wall-Mounted Hump with Separation and Reattachment, AIAA Journal, Vol. 56, 2018, pp. 715 730.

[17] Matai, R., and Durbin, P., Large-eddy simulation of turbulent ow over a parametric set of bumps, Journal of Fluid Mechanics, Vol. 866, 2019, pp. 503 525.

[18] Peters, E. L., Balin, R., Jansen, K. E., Doostan, A., and Evans, J. A., S-Frame discrepancy correction models for data-informed Reynolds stress closure, arXiv:2004.08865 [physics. u-dyn], 2020.

[19] Greenblatt, D., Paschal, K. B., Yao, C.-S., Harris, J., Schae er, N. W., and Washburn, A. E., Experimental investigation of separation control Part 1: Baseline and steady suction, AIAA Journal, Vol. 44, 2006, pp. 2820 2830.

[20] Postl, D., and Fasel, H. F., Direct Numerical Simulation of Turbulent Flow Separation from a Wall-Mounted Hump, AIAA Journal, Vol. 44, No. 2, 2006, pp. 263 272. https://doi.org/10/d3jr65.

[21] You, D., Wang, M., and Moin, P., Large-eddy simulation of ow over a wall-mounted hump with separation control, AIAA Journal, Vol. 44, 2006, pp. 2571 2577.

[22] Park, G. I., and Moin, P., "Wall-modeled LES: Recent applications to complex flows," *Center for Turbulence Research Annual Research Briefs 2016*, 2016, pp. 39–50.

[23] Webster, D. R., DeGraaff, D. B., and Eaton, J. K., "Turbulence characteristics of a boundary layer over a two-dimensional bump," *Journal of Fluid Mechanics*, Vol. 320, 1996, pp. 53–69.

[24] Slotnick, J. P., "Integrated CFD Validation Experiments for Prediction of Turbulent Separated Flows for Subsonic Transport Aircraft," *STO-MP-AVT-307*, 2019.

[25] Williams, O., Samuell, M., Sarwas, E. S., Robbins, M., and Ferrante, A., "Experimental Study of a CFD Validation Test Case for Turbulent Separated Flows," *AIAA Scitech 2020 Forum*, Orlando, 2020.

[26] Uzun, A., and Malik, M. R., "Simulation of a Turbulent Flow Subjected to Favorable and Adverse Pressure Gradients," *AIAA Aviation 2020 Forum*, 2020. https://doi.org/10/ggz8dg.

[27] Balin, R., and Jansen, K. E., "Direct numerical simulation of a turbulent boundary layer with strong pressure gradients," *arXiv:2010.08577 [physics.flu-dyn]*, 2020.

[28] Lilly, D. K., "A proposed modification of the Germano subgrid-scale closure method," *Physics of Fluids*, Vol. 4, 1992, pp. 633–635.

[29] Meneveau, C., and Lund, T. S., "The Dynamic Smagorinsky Model and Scale-Dependent Coefficients in the Viscous Range of Turbulence," *Physics of Fluids*, Vol. 9, No. 12, 1997, pp. 3932–3934. https://doi.org/10/ct4tq5.

[30] Shur, M. L., Spalart, P. R., Strelets, M. K., and Travin, A. K., "Synthetic turbulence generators for RANS-LES interfaces in zonal simulations of aerodynamic and aeroacoustic problems," *Flow, Turbulence and Combustion*, Vol. 93, 2014, pp. 63–92.

[31] Shur, M. L., Spalart, P. R., Strelets, M. K., and Travin, A. K., "A hybrid RANS-LES approach with delayed-DES and wall-modelled LES capabilities," *International Journal of Heat and Fluid Flow*, Vol. 29, 2008, pp. 1638–1649.

[32] Spalart, P. R., Belyaev, K. V., Garbaruk, A. V., Shur, M. L., Strelets, M. K., and Travin, A. K., "Large-eddy and direct numerical simulations of the Bachalo-Johnson flow with shock-induced separation," *Flow, Turbulence and Combustion*, Vol. 99, 2017, pp. 865–885.

[33] Balin, R., Jansen, K. E., and Spalart, P. R., "Wall-Modeled LES of Flow over a Gaussian Bump with Strong Pressure Gradients and Separation," *37th AIAA Applied Aerodynamics Conference*, 2020.

[34] Spalart, P. R., and Allmaras, S. R., "A one-equation turbulence model for aerodynamic flows," *Recherche Aerospatiale*, Vol. 1, 1994, pp. 5–21.

[35] Patterson, J. W., Balin, R., and Jansen, K. E., "Assessing and Improving the Accuracy of Synthetic Turbulence Generation," *Journal of Fluid Mechanics*, Vol. 906, 2021. https://doi.org/10/ghj99p.

[36] Whiting, C. H., and Jansen, K. E., "Stabilized Finite Element Methods For Fluid Dynamics Using A Hierarchical Basis," Ph.D. thesis, Rensselaer Polytechnic Institute, 1999.

[37] Jansen, K. E., Whiting, C. H., and Hulbert, G. M., "Generalized-α method for integrating the filtered Navier-Stokes equations with a stabilized finite element method," *Computer Methods in Applied Mechanics and Engineering*, 2000. https://doi.org/10.1016/S0045-7825(00)00203-6.

[38] Spalart, P. R., "Detached-eddy simulation," *Annual Review of Fluid Dynamics*, Vol. 41, 2009, pp. 181–202.

[39] Smits, A. J., Matheson, N., and Joubert, P. N., "Low-Reynolds-Number Turbulent Boundary Layers in Zero and Favorable Pressure Gradients." *Journal of Ship Research*, Vol. 27, 1983, p. 11.

[40] Schlatter, P., Li, Q., Brethouwer, G., Johansson, A. V., and Henningson, D. S., "Structure of a Turbulent Boundary Layer Studied by DNS," *Direct and Large-Eddy Simulation VIII*, edited by H. Kuerten, B. Geurts, V. Armenio, and J. Fröhlich, Springer Netherlands, 2011, pp. 9–14.

[41] Coles, D. E., "The Turbulent Boundary Layer in a Compressible Fluid," Tech. Rep. R-403-PR, USAF The Rand Corporation, 1962.

[42] Prakash, A., Jansen, K. E., and Evans, J. A., "Optimal Clipping of the Gradient Model for Subgrid Stress Closure," *AIAA Scitech 2021 Forum*, 2021.

[43] Sayadi, T., and Moin, P., "Large Eddy Simulation of Controlled Transition to Turbulence," *Physics of Fluids*, Vol. 24, No. 11, 2012. https://doi.org/10/gbb9km.

[44] Shur, M. L., Strelets, M. K., Travin, A. K., and Spalart, P. R., "Turbulence modeling in rotating and curved channels: assessing the Spalart-Shur correction," *AIAA Journal*, Vol. 38, 2000, pp. 784–792.

[45] Travin, A. K., Shur, M. L., Spalart, P. R., and Strelets, M. K., "Improvement of delayed detached-eddy simulation for LES with wall modelling," *European Conference on Computational FLuid Dynamics ECCOMAS CFD 2006*, TU Delft, 2006.

[46] Porte-Agel, F., Meneveau, C., and Parlange, M. B., "A Scale-Dependent Dynamic Model for Large-Eddy Simulation: Application to a Neutral Atmospheric Boundary Layer," *Journal of Fluid Mechanics*, Vol. 415, 2000, pp. 261–284. https://doi.org/10/cjbgm5.

[47] Meneveau, C., "Germano Identity-Based Subgrid-Scale Modeling: A Brief Survey of Variations on a Fertile Theme," *Physics of Fluids*, Vol. 24, No. 12, 2012. https://doi.org/10/gbccz9.